

# SPECTRA FROM FORMING REGION OF THE FIRST GALAXIES : THE EFFECT OF ASPHERICAL DECELERATION

Masakazu AR. Kobayashi and Hideyuki Kamaya

*Department of Astronomy, School of Science, Kyoto University, Sakyo-ku, Kyoto 606-8502, JAPAN*

TO: MARK: kobayasi@kusaastro.kyoto-u.ac.jp

## ABSTRACT

$\text{Ly}\alpha$  line emission from the Loeb-Rybicki (LR) halo, which is the expanding HI IGM (intergalactic medium) around the first star clusters and the ionized interstellar medium, is investigated by solving a radiative transfer problem. While the initial scattering optical depth is  $\sim 10^5$  for the  $\text{Ly}\alpha$  photons, most of the  $\text{Ly}\alpha$  photons can escape when the cumulative frequency-shift due to the expansion of the HI IGM becomes significantly large. The current paper improves upon previous treatments of the scattering processes and the opacity for the  $\text{Ly}\alpha$  transfer. Confirming the previous results of the LR halo, we investigate the effect of the aspherical expansion of the IGM. The asphericity is hypothesized to follow the initial stage of the gravitational deceleration to form the large scale filamentary structure of the Universe. According to our results, the effect of the asphericity lets the peak wavelength of the line profile shift to longer wavelengths and the FWHM of the profile become wider than those of the spherically expanding model. To detect these features is meaningful if we are interested in the initial evolution of the large scale structure, since they reflect the dynamical properties of the IGM at that time. Furthermore, given the recent discovery of the high redshift cosmological reionization, we briefly comment on the effects of the redshift and the cosmological parameters on the line profile.

*Subject headings:* line: profiles — radiative transfer — galaxies: intergalactic medium — galaxies: formation

## 1. INTRODUCTION

The epoch of cosmic reionization is one of the most important epochs to understand in the investigation of the history of the universe, because it contains the imprint of important

information on cosmic structure formation and evolution. This is because the reionization of the intergalactic medium (IGM) occurs promptly (e.g. Gnedin & Ostriker 1997) and the cosmic ionizing background radiation can penetrate the dense HI condensations of virialized objects (Miralda-Escudé, Haehnelt, & Rees 2000; Barkana & Loeb 1999).

The epoch of the reionization observationally relates to the Gunn-Peterson trough (Gunn & Peterson 1965). The significantly ionized IGM in the observed spectra of QSOs at  $z < 5.6$  (Dey et al. 1998; Hu, Cowie, & McMahon 1998; Spinrad et al. 1998; Weymann et al. 1998) implies that most of the intergalactic hydrogen in the Universe has been reionized before  $z \sim 5.6$ . Some standard cosmological models predict that reionization takes place around a redshift of  $z \sim 6$ . However, according to the results of the WMAP project, Kogut et al. (2003) may have discovered the high redshift reionization of the Universe ( $z \sim 20$ ). To resolve this discrepancy, the direct detection of the emission from the first objects is very important. This is because that emission reflects the physical and chemical properties of the first star clusters (Shchekinov 1991; Kamaya & Silk 2002) and/or protogalaxies. Once we know the origin of the first emission, the ionization rate at that time is investigated. Therefore, new detailed studies and confirmation of the previous studies of the first emission in another way are important for the subsequent progress of the research fields.

It is interesting to detect just the first Ly $\alpha$  photons since the star formation rate and/or the ionization structure of the interstellar medium are examined from that intensity. Using standard cosmological models, cosmic recombination takes place at  $z \sim 10^3$ . After that epoch, the Universe becomes predominantly neutral. When the first galaxies and/or star clusters form, they are surrounded by the neutral IGM. One might naively expect the damping wing of the Ly $\alpha$  trough to eliminate any trace of a Ly $\alpha$  emission line in the observed source spectra. However, the Ly $\alpha$  photons are scattered and diffused redward in frequency owing to the Hubble expansion of the surrounding HI IGM (Loeb & Rybicki 1999 ; hereafter LR99). When the cumulative frequency-shift becomes significantly large, they can escape and travel freely toward the observer.

Although we investigate a similar problem to that in LR99, the radiative transfer model is improved in the two ways : (1) Formulation of the geometrical scattering (i.e. test photons scatter spatially three dimension); and (2) Formulation of the Ly $\alpha$  opacity. Thanks to these two improvements and the confirmation of the previous studies, we can study more complex physical conditions in the expanding HI gas. Since the large scale structure (LSS) forms filaments, this suggests the initial stage of the gravitational deceleration for the LSS favors an asymmetrical expansion of the HI halo. Indeed, the inhomogeneity of the self-gravitating system can grow in a free-fall time (e.g. Lin, Mestel, & Shu 1965). As long as the expansion time-scale is comparable to the free-fall time scale, the asymmetrical deceleration of the

IGM occurs in the time-scale of the Hubble expansion, although the initial asymmetry is obviously very weak. As the first and the simplest hypothesis to investigate the effect of the inhomogeneity via the gravitational deceleration for the LSS formation, we adopt the aspherical expansion model of HI IGM. The physical implication drawn from the current analysis will suggest to us further research projects for the first Ly $\alpha$ . Since the lumpiness and/or small-scale irregularity may be important for a realistic treatment of the first Ly $\alpha$ , we will investigate these effects in subsequent papers.

This paper is organized as follows: In §2 we describe the formalism of the Ly $\alpha$  line transfer problem commenting on the differences between our approach and LR99. In §3 we outline our Monte Carlo simulation method. In §4 we discuss our numerical results including the effects of a more complete representation of the Ly $\alpha$  opacity, the effect of asphericity in the expanding IGM, and the sensitivity of our results to redshift and cosmological parameters. In §5 we summarize our study.

## 2. FORMULATION

We formulate the problem according to LR99, while the HI IGM is hypothesized to expand aspherically. In general, the exactly spherical expansion is not expected as long as the IGM decelerates to form LSS. This is recognized because the free-fall time,  $t_{ff}$ , is comparable to the Hubble expansion time,  $t_h$ , as explained in §1. Then, to find the effect of the asymmetry, we shall set the most simple assumption to the recession velocity, *spheroidal expansion*:  $v = H_s [\varepsilon^2 (x^2 + y^2) + z^2]^{1/2}$ , where  $v$  is recession velocity,  $H_s$  is the Hubble expansion rate at the source redshift of  $z_s$ , and  $\varepsilon$  is *ellipticity* or decreasing rate of the recession velocity to the pure Hubble expansion. We shall estimate the allowed order of  $\varepsilon$ . The ratio of the two time-scales is denoted as

$$\frac{t_{ff}}{t_h} \sim \frac{\pi}{2} \Omega_M^{-1/2} \delta^{-1/2}. \quad (1)$$

Here,  $\delta$  is the ratio of the density of the halo to the mean density of the Universe at  $z$ . Of course, this ratio must not be different from unity very much as long as IGM expands. Since the density of the aspherically decelerating HI halo is larger than that of the spherically expanding halo, we find  $\delta = 1/\varepsilon$  with mass conservation. Fixing the ratio of Eq.(1) to be unity and postulating  $\delta \sim 6$ , for example, we estimate  $\varepsilon \sim 0.2$  for  $\Omega_M = 0.4$ . Thus, we recognize that order of  $\varepsilon$  is about 0.1. The case of  $\varepsilon = 0.1$  is considered as an extreme case. Obviously,  $\varepsilon = 1$  corresponds to LR99.

Although  $\varepsilon$  should approach to unity differentially from small scale to large scale, we assign  $\varepsilon$  a single value for simplicity. Fortunately, the size of the concerned region,  $\sim r_*$ ,

which is a characteristic distance from the Ly $\alpha$  photon source as defined later, is  $\sim$  Mpc as estimated in LR99. That is,  $r_*$  corresponds to the size of groups of galaxies and the region at  $r_*$  can be regarded as decelerating region although the allowed deceleration should be small (but not zero). Expansion law of the spheroid approaches to that of the spherical model at larger scale than  $r_*$ . Properties of test photons are also determined at  $\sim r_*$ . Hence, the single value hypothesis for  $\varepsilon$  can present the physical insight into the effect of the deceleration for the LR halo. In realistic condition, by the way,  $\varepsilon$  inside  $r_*$  should decrease toward the center differentially. Then, our finding characteristic effect of the deceleration may be enhanced because the number of scattering can increase owing to the deceleration as shown in this paper.

Let  $I = I(\nu, \mathbf{\Omega}, \mathbf{r})$  be the specific intensity (in photons  $\text{cm}^{-2} \text{s}^{-1} \text{sr}^{-1} \text{Hz}^{-1}$ ), where  $\nu$  is comoving frequency,  $\mathbf{r} = (x, y, z)$  is the radial vector from the source galaxy, and  $\mathbf{\Omega}$  is the scattering direction. The spatial components of the direction cosines of  $\mathbf{\Omega}$  are  $(u, v, w)$ , respectively. With the assumption of isotropic coherent scattering, the comoving transfer equation for a resonance line is given by

$$\mathbf{\Omega} \cdot \nabla I + \alpha \psi(\varepsilon, w) \frac{\partial I}{\partial \nu} = \chi_\nu (J - I) + S. \quad (2)$$

Here,  $\nu$  is the shift of the frequency  $\nu_\alpha - \nu_{\text{photon}}$  where  $\nu_\alpha$  is the resonant frequency and  $\nu_{\text{photon}}$  is the photon frequency;  $\chi_\nu$  is the scattering opacity at  $\nu$  (eq. (4) in LR99);  $J = (1/2) \int_{-1}^1 I d\mu$  is the mean intensity;  $S$  is the emission function (in photons  $\text{cm}^{-3} \text{s}^{-1} \text{sr}^{-1} \text{Hz}^{-1}$ , eq. (3) in LR99);  $\alpha \equiv H_s \nu_\alpha / c$  is the increasing rate of the frequency shift per unit distance in the spherically expanding IGM (eq. (2) in LR99); and

$$\psi(\varepsilon, w) = [\varepsilon^2 + (1 - \varepsilon^2) w^2]^{1/2} \quad (3)$$

represents the effect of aspherical expansion.

In LR99 the scattering opacity  $\chi_\nu$  was approximated as  $\chi_\nu \sim \beta/\nu^2$ . In the current paper, we formulate the opacity in the following more complete form:

$$\chi_\nu = \frac{\beta/\varepsilon}{\Lambda_\alpha^2/16\pi^2} \quad \text{for } \nu^2 \ll \Lambda_\alpha^2/16\pi^2, \quad (4)$$

$$= \frac{\beta/\varepsilon}{\nu^2 + \Lambda_\alpha^2/16\pi^2} \quad \text{for } \nu^2 \sim \Lambda_\alpha^2/16\pi^2, \quad (5)$$

$$= \frac{\beta/\varepsilon}{\nu^2} \quad \text{for } \Lambda_\alpha^2/16\pi^2 \ll \nu^2 \text{ \& } \nu \ll \nu_\alpha, \quad (6)$$

$$= \left(1 - \frac{\nu}{\nu_\alpha}\right)^4 \frac{\beta/\varepsilon}{\nu^2} \quad \text{for } \nu \sim \nu_\alpha, \quad (7)$$

$$= 0 \quad \text{for } \nu > \nu_\alpha, \quad (8)$$

where  $\nu_\alpha = 2.47 \times 10^{15}$  Hz is the Ly $\alpha$  frequency,  $\Lambda_\alpha = (8\pi^2 e^2 f_\alpha / 3m_e c \lambda_\alpha^2) = 6.26 \times 10^8 \text{ s}^{-1}$  is the rate of spontaneous radiative decay from  $2p$  to  $1s$  energy levels of hydrogen,  $f_\alpha = 0.4162$  is the oscillator strength,  $\lambda_\alpha = 1216 \text{ \AA}$  is the wavelength of the Ly $\alpha$  line, and  $\beta$  is  $1.5\Omega_b h_0^2 (1 + z_s)^3 \text{ cm}^{-1} \text{ Hz}^2$  (eq. (5) in LR99). In the initial scattering phase, Eq.(4) is important since the frequency shift can be smaller than  $\Lambda_\alpha/4\pi$ . When the photon diffuses and the frequency shift is comparable to  $\nu_\alpha$ , Eq.(7) must be adopted as  $\chi_\nu$ .

We normalize the frequency shift and radius by convenient quantities like LR99. An appropriate frequency scale,  $\nu_*$ , is estimated from  $\tau_\nu \sim 1$ . Here,  $\tau_\nu$  is the Ly $\alpha$  optical depth from the source to the observer, and is defined as

$$\tau_\nu = \int_0^\infty \chi_{\nu+\alpha\psi r} dr. \quad (9)$$

The characteristic frequency shift of  $\nu_*$  is measured along the direction of  $z$  (i.e.  $w = 1$ ). Eq. (9) with Eq.(7) can be described as

$$\int_0^{l_0} \left(1 - \frac{\nu_* + \alpha r}{\nu_\alpha}\right)^4 \frac{\beta/\varepsilon}{(\nu_* + \alpha r)^2} dr = 1, \quad (10)$$

where  $l_0 \equiv (\nu_\alpha - \nu_*)/\alpha$  is a characteristic distance for the photon frequency to reach zero. We note that  $\nu_*$  always depends on  $\beta$  and  $\varepsilon$ . The appropriate radius, where the frequency-shift due to the Hubble expansion produces the frequency shift of  $\nu_*$ , is given by  $r_* = \nu_*/\alpha$ . For example, with  $\varepsilon = 1$ , we find  $\nu_* = 9.64 \times 10^{12} \text{ Hz}$  and  $r_* = 0.77 \text{ Mpc}$  at  $z_s = 10$  with a set of cosmological parameters of  $\Omega_b = 0.05$ ,  $\Omega_M = 0.4$ ,  $\Omega_\Lambda = 0.6$ , and  $h_0 = 0.65$ .<sup>1</sup> The normalized frequency shift  $\tilde{\nu}$  and distance  $\tilde{r}$  are then defined to be  $\tilde{\nu} \equiv \nu/\nu_*$  and  $\tilde{r} \equiv r/r_*$ .

For the reader's convenience, we present the Lyman $\alpha$  opacity  $\chi_\nu \text{ cm}^{-1}$  in Fig.1 as a function of  $\tilde{\nu}$ . The solid line denotes our  $\chi_\nu$ , and the dashed line denotes the previously adopted one from LR99. According to the definition of  $\tilde{\nu}$ , the photon frequency  $\nu_{\text{photon}}$  becomes small as  $\tilde{\nu}$  increases and reaches zero at  $\tilde{\nu} = \nu_\alpha/\nu_* \sim 2.56 \times 10^2$ . At  $\tilde{\nu} = 0$ , the frequency of the photon is the Ly $\alpha$  frequency  $\nu_\alpha$ . The differences depicted in the figure 1 are reflected in our results, while they are usually small.

---

<sup>1</sup>We adopt these cosmological parameters because of the comparison to LR99. Although the recent results of WMAP present slightly different cosmological parameters (Spergel et al. 2003), fortunately our results are not altered very much as shown in §4.4.

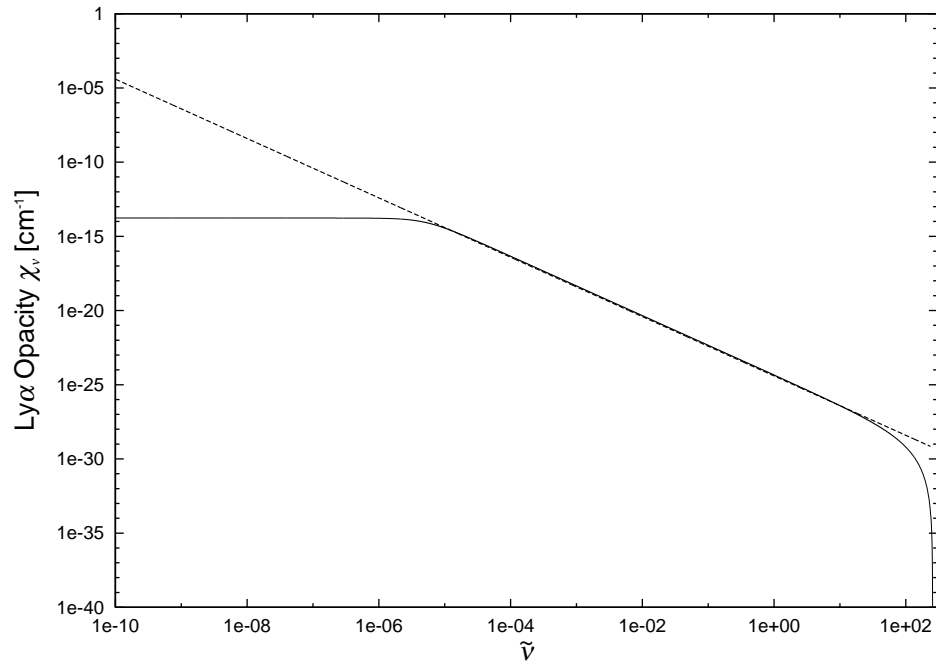


Fig. 1.— Ly $\alpha$  opacities are presented. Solid line represents the fully formulated opacity [Eq.(4) in LR99], and dashed line does the approximated opacity in LR99.

### 3. Algorithm of the Calculation

LR99 solved a dimensionless transfer equation in the diffusion regime, which is valid in the region  $\tilde{\nu} \gg \tilde{r}$ . They also studied the numerical solution of the transfer equation using a Monte Carlo technique and found that it agreed with the diffusion equation in the low frequency shift region. We also solve the transfer equation numerically by using a Monte Carlo method very similar to LR99. The number of test photons is  $10^8$ , the same as in LR99, and permits us to compare our results directly to theirs. During the calculation two photon decay is always neglected since it is difficult to destroy the Lyman  $\alpha$  photons transferred in the surrounding HI. This is because the event rate of two photon decay is determined by the process of a transition between  $2s$  -  $2p$  owing to the radiative collision with an electron (Breit & Teller 1940; Spitzer & Greenstein 1951). As long as the relic electron number density is very small, the event rate of two photon decay should be negligible.

LR99 adopted the initial shift method in the first step of each simulation. That is, the initial shift of  $\tilde{\nu}$  is 0.01 and  $\tilde{r}$  is determined stochastically by means of the diffusion solution of LR99. We have confirmed independently that the initial shift method is very reasonable. This is because the initial optical depth is always much larger than unity. Hence we also adopt that method in all first time steps of the simulations.

#### 1. 3D scattering

LR99 assumed isotropic, coherent scattering through a spherically symmetric, neutral medium such that the scattering could be described by a single angular parameter  $\mu = \cos \theta$  relative to the radius  $r$ . We generalize to three dimensional scattering. The scattering processes in 3D coordinates is described by two parameters of  $\mu = 2R_1 - 1$  and  $\phi = \pi(2R_2 - 1)$ . Here,  $\phi$  is the change in azimuth, and  $R_1$  and  $R_2$  are random numbers on the interval of  $(0, 1)$ . Defining  $\mu$  as  $\cos \alpha$ , we measure  $\alpha$  in the plane determined by the old and new photon paths.

The direction cosines of  $u_{i+1}, v_{i+1}, w_{i+1}$  after the scattering are determined by using the direction cosines of the incident photon,  $u_i, v_i, w_i$ :

$$\begin{aligned} u_{i+1} &= \sin \alpha (\cos \phi w_i u_i - \sin \phi v_i) / (1 - w_i^2)^{1/2} + \cos \alpha u_i, \\ v_{i+1} &= \sin \alpha (\cos \phi w_i v_i + \sin \phi u_i) / (1 - w_i^2)^{1/2} + \cos \alpha v_i, \\ w_{i+1} &= -\sin \alpha \cos \phi (1 - w_i^2)^{1/2} + \cos \alpha w_i. \end{aligned} \quad (11)$$

As  $|w_i|$  approaches unity, according to Witt (1977), the set of equations (11) breaks down and is replaced by

$$u_{i+1} = \sin \alpha \cos \phi, \quad v_{i+1} = \sin \alpha \sin \phi, \quad w_{i+1} = \cos \alpha w_i \quad \text{for } 1 - |w_i| \leq 10^{-10}. \quad (12)$$

## 2. Opacity selection

LR99 used a single approximate form for the opacity as a function of frequency (i.e. our equation (6) for  $\varepsilon = 1$ ). We use the more complete form for the opacity by Equations (4-8). Selecting the appropriate opacity in Eqs.(4-8) according to  $\tilde{\nu}$ , we evaluate the path length along the ray,  $\tilde{l}$ , and the maximum optical depth:  $\tau_{\max} \equiv \int_0^\infty \chi_{\nu+\alpha\psi l} dl$ . Once the optical depth  $\tau$  for a test photon becomes larger than the maximum optical depth  $\tau_{\max}$ , we say that it escapes from the LR halo. Here,  $\tau$  is determined as  $-\ln R_{\text{sca}}$  where  $R_{\text{sca}}$  is a random number between zero and one.

## 3. Aspherical expansion

LR99 assumed that the neutral IGM surrounding the Ly $\alpha$  point source undergoes uniform Hubble expansion. Locally we do not expect this to be the case. The cumulative frequency-shift and  $\tau_{\max}$  differ depending on the scattering direction. According to Eq.(3), the increment of the frequency shift of the scattering photon is represented by

$$\tilde{\nu}_{i+1} = \tilde{\nu}_i + \psi(\varepsilon, w_i) \tilde{l}. \quad (13)$$

# 4. Results

We first compare the results of our 3D simulation technique and improved approximation to the Ly $\alpha$  opacity to those of LR99. We then expand upon that previous work by considering the aspherical expansion of the IGM. Recently Spergel et al. (2003) have used WMAP data to determine more precise values for the cosmological model parameters. WMAP data also suggest that the epoch of reionization may be at a redshift larger than 10 (Kogut et al. 2003). Thus we conclude with a discussion of the effect of redshift and the cosmological model parameters on the observable Ly $\alpha$  line profile.

All figures presenting the results are made by counting the number of escape photons in the same interval of normalized frequency shift of  $\tilde{\nu}$  in log scale. We choose the interval of  $10^{-3}$  from  $\log \tilde{\nu} = -1.0$  to 2.0. For a clear presentation of the effect of the aspherical expansion, we count the photons all over the complete solid angle of  $4\pi$ .

## 4.1. Geometrical effect

In Fig.2 the geometrical effect of using our 3D numerical method for the scattering is compared to the 2D treatment of LR99. The same scattering coefficient used in LR99 is adopted with  $\varepsilon = 1$ . The horizontal axis is the normalized frequency,  $\tilde{\nu}$ , and the vertical axis



is the escape fraction of test photons. The 2D treatment of scattering by LR99 is the solid line; while our 3D treatment of the scattering is the dashed line. We observe no difference between the lines. This agreement comes from a simple approximation that the neutral IGM around the  $\text{Ly}\alpha$  source has spherical symmetry. Furthermore, it shows our 3D scheme has sufficient resolution to compare directly with the results of LR99. Hereafter, we compare our results with the spherically symmetric case in 3D coordinates, which is called *3D LR99*.

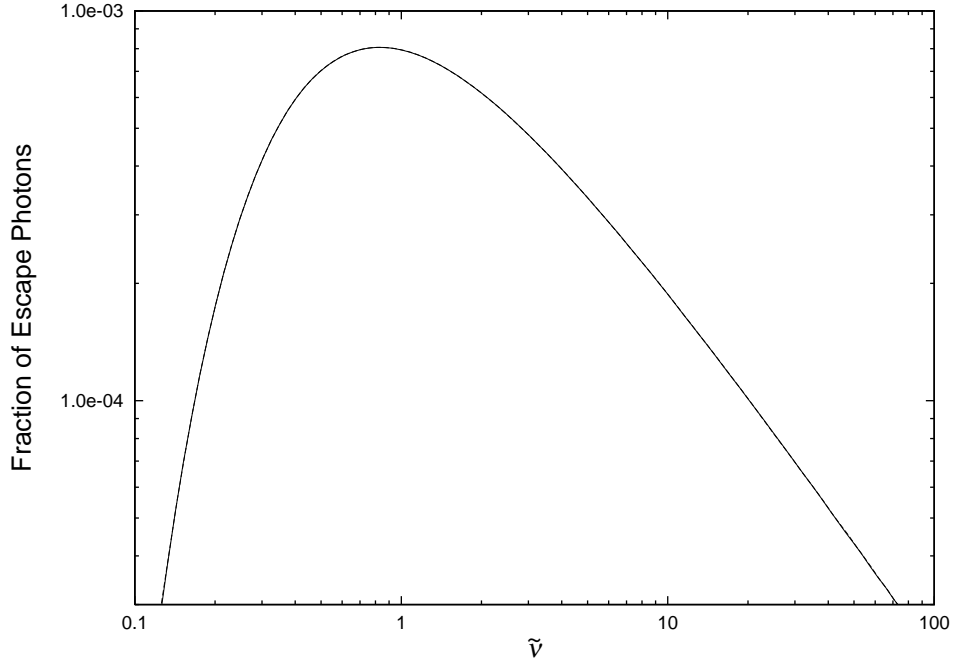


Fig. 2.— Confirmation of our scheme. Solid line is the spatially 2D scattering model and dashed line is the spatially 3D scattering model.

#### 4.2. Opacity evaluation effect

How about the effect of opacity? Fig.3 shows the results with the fully formulated opacity and  $\varepsilon = 1$  (*solid line*) and that of 3D LR99 (*dashed line*), using the same definition of both coordinates as in figure 2. It is found that there are almost no difference between the line profiles of ours and LR99’s. This result confirms that the  $\text{Ly}\alpha$  opacity is approximated well in LR99.

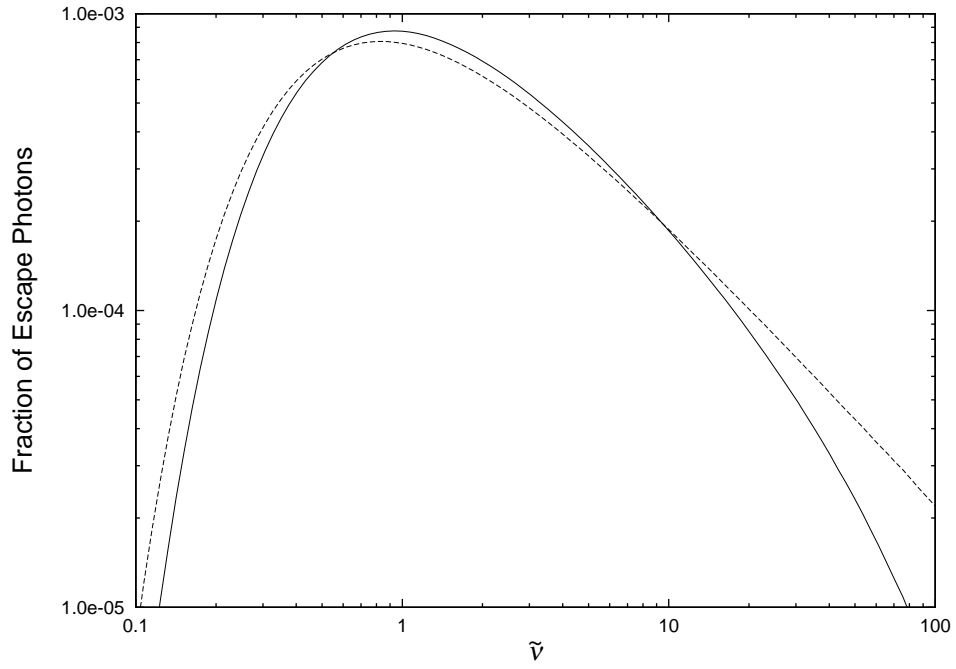


Fig. 3.— The effect of the selection of opacity is depicted. Fully formulated opacity is presented as the solid line ( $\epsilon = 1$ ) and 3D LR99 is the dashed line.

Transforming  $\tilde{\nu}$  to the observational wavelength of  $\lambda_{\text{obs}}$  by

$$\lambda_{\text{obs}} = (1 + z_s) \lambda_{\alpha} \left[ 1 - \left( \frac{\nu_*}{\nu_{\alpha}} \right) \tilde{\nu} \right]^{-1}, \quad (14)$$

we compare our model with 3D LR99. In Eq.(14), the term  $[1 - (\nu_*/\nu_{\alpha}) \tilde{\nu}]^{-1}$  represents the effect of the cumulative frequency-shift. The bin of the wavelength for photon counts corresponds to that of the frequency. We show the normalized luminosity of the Ly $\alpha$  line per unit wavelength,  $\tilde{L}_{\alpha}(\lambda)$ , in Fig.4. This can be converted into the observational  $L_{\alpha}(\lambda)$  by multiplying the steady emission rate of Ly $\alpha$  photons at the source,  $\dot{N}_{\alpha}$  (in photons  $s^{-1}$ ), by the Ly $\alpha$  photon energy,  $h\nu_{\alpha}$ . The observed Ly $\alpha$  wavelength emitted at  $z_s = 10$  is  $\lambda_{\text{obs}} =$

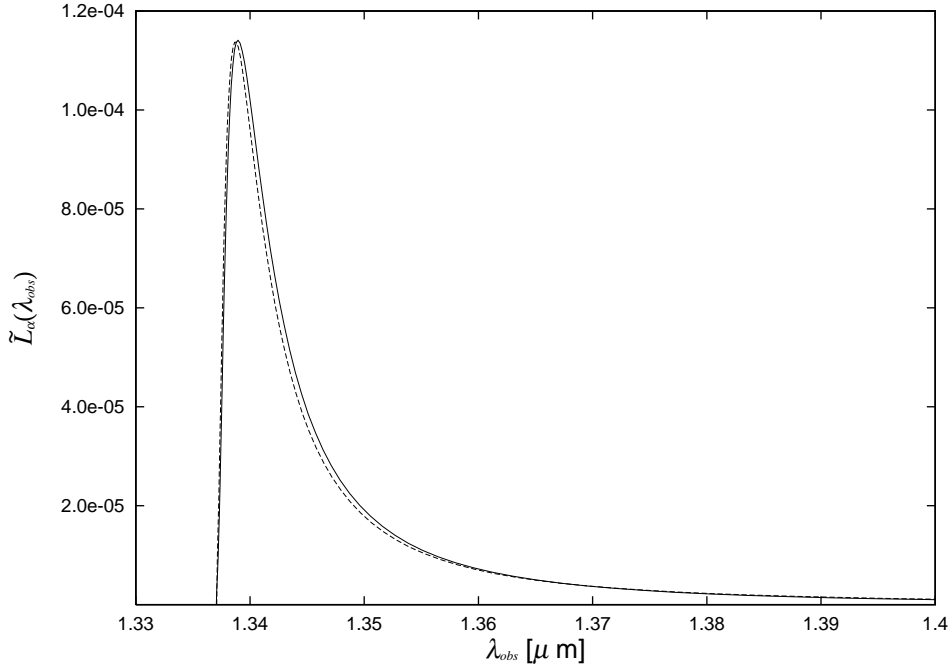


Fig. 4.— Normalized luminosities of the Ly $\alpha$  line profile as a function of observational wavelength  $\lambda_{\text{obs}}$  [ $\mu\text{m}$ ] are depicted. Our result is solid line ( $\varepsilon = 1$ ) and 3D LR99 is dashed line.

1.337  $\mu\text{m}$ . As shown in the figure, the peaks of the line profiles shift to  $\lambda_{\text{peak}} \sim 1.339 \mu\text{m}$ . This shift from the line center is  $\sim 2 \text{ nm}$ . We need a wavelength resolution of  $R \sim 7.8 \times 10^2$  if it is to be detected. The full widths at half maximum (FWHM) of our line profile and 3D LR99 are  $5.27 \times 10^{-3} \mu\text{m}$  and  $4.94 \times 10^{-3} \mu\text{m}$ , respectively.

### 4.3. Aspherical expansion effect

In this section the effect of the aspherical expansion of the HI IGM is summarized. Fig.5 presents the normalized luminosities of Ly $\alpha$  line profiles for various values of the parameter  $\varepsilon$  that characterizes the asphericity of the IGM. Here, the solid line is  $\varepsilon = 1.0$ , long dashed line is  $\varepsilon = 0.9$ , short dashed line is  $\varepsilon = 0.7$ , dotted line is  $\varepsilon = 0.5$ , long dash-dotted line is  $\varepsilon = 0.3$ , and short dash-dotted line is  $\varepsilon = 0.1$ . What is the distinct property of the line

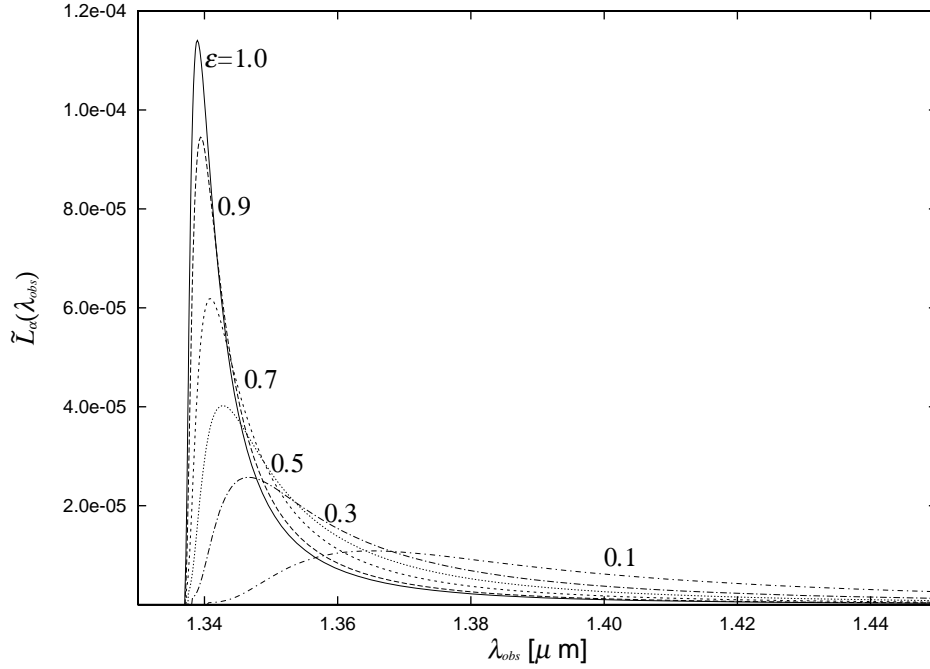


Fig. 5.— The effect of the aspherical expansion is presented. Each of the lines shows  $\varepsilon = 1.0$  (solid line;  $\varepsilon = 0.9$  (long dashed line),  $\varepsilon = 0.7$  (short dashed line),  $\varepsilon = 0.5$  (dotted line),  $\varepsilon = 0.3$  (long dash-dotted line), and  $\varepsilon = 0.1$  (short dash-dotted line), respectively.

profile with  $\varepsilon \neq 1.0$ ? The characteristic quantities are summarized in Table 1, where some results of other  $\varepsilon$ 's are also presented. The last column in Table 1 is the necessary resolution to distinguish  $\lambda_{\text{peak}}$  from the Ly $\alpha$  line center of  $(1 + z_s)\lambda_\alpha$ .

According to table 1, the distinct effects of the asphericity are the shift of the peak and the broadening of the FWHM of the line profiles. These are clearly seen in the line profile with  $\varepsilon = 0.1$ . If there is strong asphericity of the expanding HI IGM, we will detect broadening of FWHM and the shift of the peak wavelength of the line profile. This could be observable with the JWST and signal the presence of the LR halo.

$\varepsilon$	FWHM	$\lambda_{\text{peak}}$	peak value	$R$
1.0	$5.27 \times 10^{-3} \mu\text{m}$	$1.3390 \mu\text{m}$	$1.14 \times 10^{-4}$	$7.8 \times 10^2$
0.9	$6.38 \times 10^{-3} \mu\text{m}$	$1.3394 \mu\text{m}$	$9.45 \times 10^{-5}$	$6.2 \times 10^2$
0.8	$7.86 \times 10^{-3} \mu\text{m}$	$1.340 \mu\text{m}$	$7.69 \times 10^{-5}$	$4.7 \times 10^2$
0.7	$9.77 \times 10^{-3} \mu\text{m}$	$1.341 \mu\text{m}$	$6.19 \times 10^{-5}$	$3.7 \times 10^2$
0.6	$1.21 \times 10^{-2} \mu\text{m}$	$1.342 \mu\text{m}$	$4.97 \times 10^{-5}$	$3.0 \times 10^2$
0.5	$1.48 \times 10^{-2} \mu\text{m}$	$1.343 \mu\text{m}$	$4.03 \times 10^{-5}$	$2.5 \times 10^2$
0.4	$1.80 \times 10^{-2} \mu\text{m}$	$1.344 \mu\text{m}$	$3.27 \times 10^{-5}$	$2.0 \times 10^2$
0.3	$2.30 \times 10^{-2} \mu\text{m}$	$1.346 \mu\text{m}$	$2.57 \times 10^{-5}$	$1.5 \times 10^2$
0.2	$3.25 \times 10^{-2} \mu\text{m}$	$1.352 \mu\text{m}$	$1.86 \times 10^{-5}$	94
0.1	$1.11 \times 10^{-2} \mu\text{m}$	$1.365 \mu\text{m}$	$1.09 \times 10^{-5}$	48

Table 1: Summary of the effect of the aspherical deceleration.

For increasing asphericity, i.e. a decreasing  $\varepsilon$ , the optical depth for photons to scatter becomes larger than in the spherical model. Thus, although the typical shift per scattering due to the expansion of the universe becomes small, the number of scattering events increases, thus increasing the probability that a photon will be shifted far from the line center.

#### 4.4. The Effect of Redshift and Cosmological Parameters

WMAP data suggest that cosmic reionization may take place at  $z_s \sim 20$  (Kogut et al. 2003). In Fig.6 we show the results of Ly $\alpha$  line transfer on the Ly $\alpha$  line profiles from a source at  $z_s = 20$  (solid line) compared to a source at  $z_s = 10$  (dashed line). The coordinates are the same as in Fig.3. We find the line profile of  $z_s = 20$  coincides with that of  $z_s = 10$  very well. This comes from the fact that most of the Ly $\alpha$  photons can escape from the IGM when their cumulative frequency shift becomes  $\sim \nu_*$ , and it takes place at the distance of  $\sim r_*$  from the source.

While  $\nu_*$  and  $r_*$  depend upon redshift, the shape of the two line profiles as functions of the normalized  $\tilde{\nu}$  are very similar. The effect of redshift is not significant except in the normalizations. This result presents the useful implication that when we examine line profiles at a variety of redshifts, it is sufficient for us to know the characteristic frequency shift and radius at each redshift. Hence, we summarize the redshift dependence of  $\nu_*$  in Fig.7. Here, the solid line is  $\nu_*$  of Eq.(10), while the dashed line is  $\nu_*^{\text{app}}$  which is adopted in LR99 and determined by Eq.(6) and Eq.(9). For simplicity, we present the cases with  $\varepsilon = 1$ . We hope these results are useful for the heterorelation of future observations.

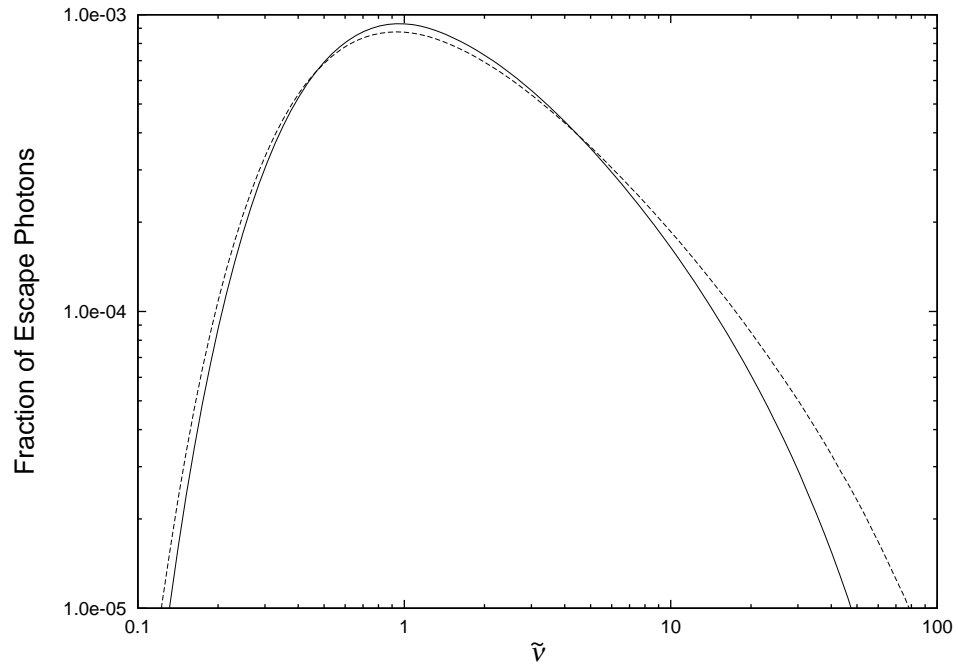


Fig. 6.— Line profiles of  $z_s = 20$  (*solid line*) and  $z_s = 10$  (*dashed line*) with  $\varepsilon = 1$  are presented.

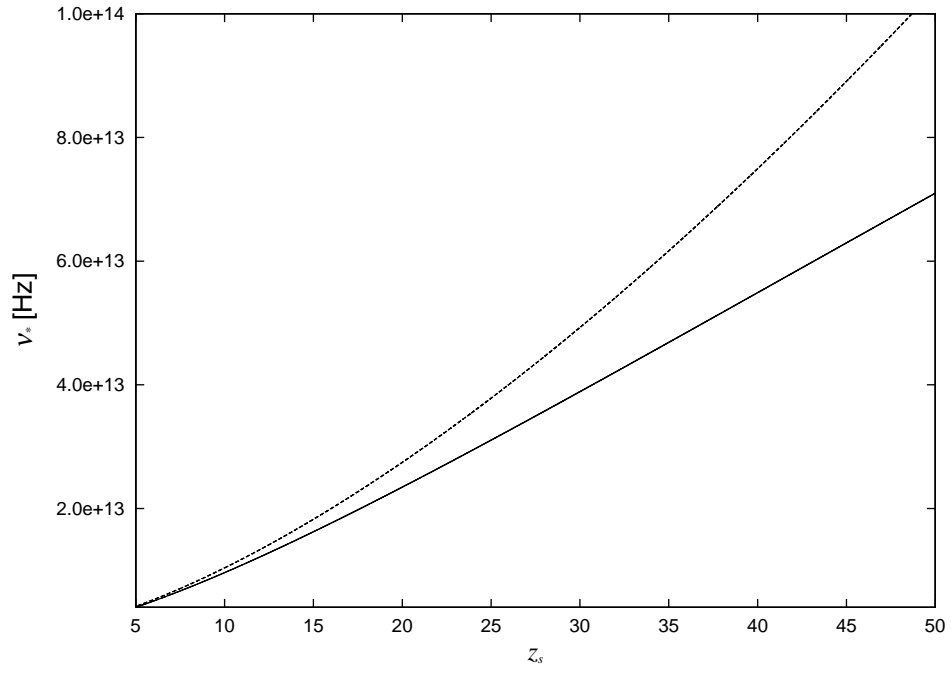


Fig. 7.— Redshift dependence of the characteristic frequency shifts is depicted. Solid line is  $\nu_*$ , and dashed line is  $\nu_*^{\text{app}}$ .

We also simulate the line transfer with the cosmological parameters found by Spergel et al. (2003) in their analysis of WMAP data, who suggest  $h_0 = 0.71_{-0.03}^{+0.04}$ ,  $\Omega_M h_0^2 = 0.135_{-0.009}^{+0.008}$ ,  $\Omega_b h_0^2 = 0.0224_{-0.009}^{+0.009}$ , and  $\Omega_\Lambda = 1.0_{-0.02}^{+0.02} - \Omega_M$ . Fig.8 presents the results at  $z_s = 10$ . The solid line adopts the cosmological parameters of LR99, while the dashed line uses those of Spergel et al. (2003). We find the effect of the cosmological parameters on the line profile is small.

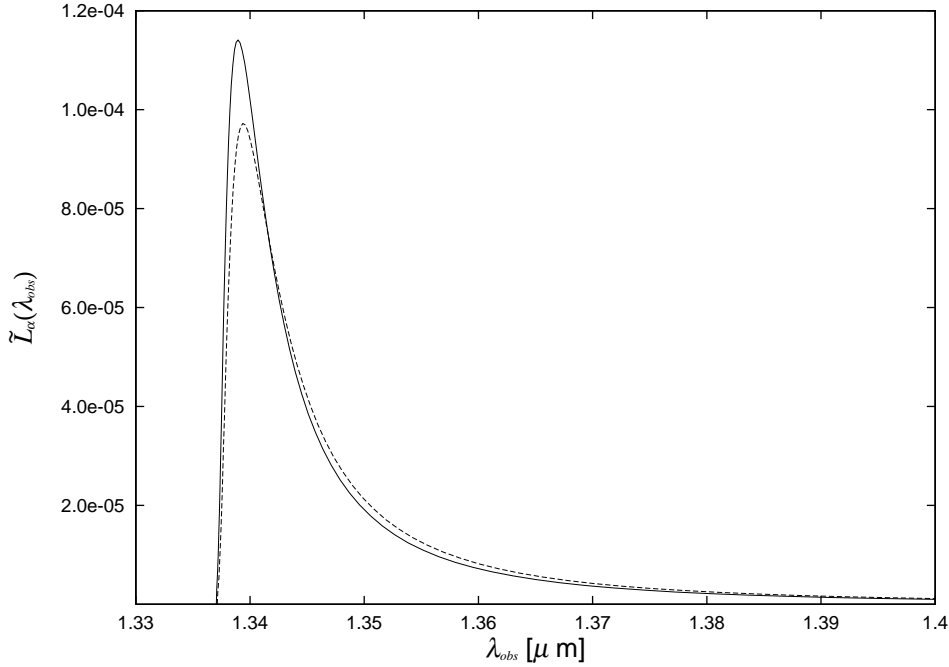


Fig. 8.— Observational line profiles at  $z_s = 10$  are presented. Solid line is the model with LR99 cosmological parameters, while dotted line is those of WMAP.

## 5. SUMMARY

In this work we extended LR99 by improving the numerical treatments of the  $\text{Ly}\alpha$  opacity and scattering processes. As part of these improvements, the effect of asphericity in the expanding IGM on the  $\text{Ly}\alpha$  profiles was examined. The results confirm LR99 very well when the aspherical deceleration is small. The effect of aspherical expansion on the line profile is reflected in a broadening of the FWHM and a shift of the peak intensity to longer wavelengths over that in the spherical model. The effect of the redshift of reionization is reflected in the normalization of the frequency shift and escape distance from the source rather than



in the shape of the normalized line ratio. Our results were insensitive to small changes in the cosmological parameters, with little difference in the results found using the cosmological model of LR99 and that derived recently from WMAP data. To detect both properties will be important to find the initial stage of the formation of LSS. Fortunately, it requires a spectroscopic resolution of  $R \sim 100 - 1000$ , which is within the design characteristics for future observational projects like JWST.

We are grateful to the referee for his/her advisable comment and excellent refereeing, which improve our paper very much in both content and presentation. We thank Profs. S. Inagaki, S. Mineshige, T. Totani for their continuous encouragement.

## REFERENCES

- Abel, T., Bryan, G. L., & Norman, M. L. 2000, *ApJ*, 540, 39
- Barkana, R. & Loeb, A. 1999, *ApJ*, 523, 54
- Breit, G., & Teller, E. 1940, *ApJ*, 91, 215
- Dey, A., Spinrad, H., Stern, D., Graham, J. R., & Chaffee, F. H. 1998, *ApJ*, 498, L93
- Gnedin, N. Y. & Ostriker, J. P., 1997, *ApJ*, 486, 581
- Gunn, J. E., & Peterson, B. A. 1965, *ApJ*, 142, 1633
- Hu, E. M., Cowie, L. L., & McMahon, R. G. 1998, *ApJ*, 502, L99
- Kamaya, H., Silk, J., 2002, *MNRAS* 332, 251
- Kogut, A., et al. 2003, *ApJS*, 148, 161
- Lin, C. C., Mestel, L., & Shu, F. H., 1965, *ApJ*, 142, 1431
- Loeb, A., & Rybicki, G. B. 1999, *ApJ*, 524, 527 (LR99)
- Miralda-Escudé, J., Haehnelt, M. & Rees, M. J. 2000, *ApJ*, 530, 1
- Shchekinov, Iu., 1991, *Ap&SS*, 175, 57
- Spergel, D. N., et al., 2003, *ApJS*, 148, 175
- Spinrad, H., Stern, D., Bunker, A., Dey, A., Lanzetta, K., Yahil, A., Pascarelle, S., & Fernández-Soto, A. 1998, *AJ*, 116, 2617

Spitzer, L. J., & Greenstein, J. L., 1951, ApJ, 114, 407

Weymann, R. J., Stern, D., Bunker, A., Spinrad, H., Chaffee, F. H., Thompson, R. I., & Storrie-Lombardi, L. J. 1998, ApJ, 505, L95

Witt, A. N. 1977, ApJS, 35, 1